

Independent Component Analysis Applied to Multielectrode Field Potential Measurements

Jarno M. A. Tanskanen^{1,2†}, Jarno E. Mikkonen¹, and Markku Penttonen¹

University of Kuopio

A. I. Virtanen Institute for Molecular Sciences

¹Department of Neurobiology, Cognitive Neurobiology Laboratory

²Department of Biomedical NMR

P.O. Box 1627, FIN-70211 KUOPIO, FINLAND

[†]Tel. +358-17-162 311, Fax: +358-17-163 030, E-mail: tanskanen@iki.fi, URL: <http://www.iki.fi/tanskanen/>

ABSTRACT

Independent component analysis (ICA) is proposed for analysis of neural population (NP) activity from electrophysiological multielectrode field potential measurements (MFPMs). The proposed analysis method provides information on spatial locations of NPs, and time lags of NP activities. In some cases, analysis results may also be interpreted as independent operational modes of NPs. In this paper, the proposed analysis method is described. The proposed analysis is demonstrated with an exemplary analysis of an in vivo MFPM from the rat hippocampus. The proposed method can be applied in analysis of any recordings of neural networks in which contributions from a number of NPs are simultaneously recorded via a number of measurement points (MPs), as well in vivo as in vitro.

1. INTRODUCTION

In this paper, we address the question of observing NPs from extracellular MFPMs. An NP is a set of neurons working in unison. FP measurements do not explicitly reveal single NP activity, but rather carry information on a mixture of the field potentials (FPs) of several NPs. We propose using ICA [1,2,3,4] to decompose MFPMs into individual NPs. We call an active NP a functional population (FUPO), and an FP produced by it a FUPO FP. Essence of the proposed analysis is to calculate ICA on several different sets of simultaneous measurements, yielding several sets of independent components (ICs). The ICs are interpreted as FUPOs, and their spatial locations are deduced by analyzing correlations of ICs from different ICAs. Since different FUPOs may carry correlated signals, ICs also may sometimes be interpreted as operational modes of the FUPOs. To interpret the ICs correctly, they must be carefully related to the neuroanatomy. Thereafter, the FUPOs can be analyzed using any appropriate methods, e.g., time-frequency and wavelet analyses [5], and current source density analyses [6]. Any brain structure, from which MFPMs can be obtained, can be subjected to ICA FUPO analysis.

In brain research, ICA has previously been applied in a multitude of cases, including electroencephalography

(EEG) [7], and EEG and magnetoencephalography (MEG) [8], and EEG, MEG, and magnetic resonance imaging analyses [9]. Better related to our work, ICA has been used, for example, in epileptiform discharge detection from EEG [10], spike train analysis of population interactions [11], and in individual neuron action potential detection [12], but to the best of our knowledge, ICA has not been previously applied in direct analysis of MFPMs. We assume, that there exist a number of FUPOs, giving rise to independent measurable FUPO FPs. Extracellular MFPMs are made amongst these FUPOs, as illustrated in Fig. 1. Each MFPM MP, i.e., measurement channel, in Fig. 1A, records a different sum of the FUPO FPs.

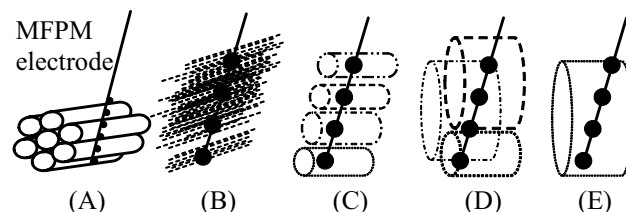


Fig. 1. (A) Illustration of an MFPM in the vicinity of FUPOs. The realization possibilities are: (B) a large number of small populations (dashed lines) in the vicinity of the MPs, (C) one population per MP, (D) each MP records contributions from one or a few FUPOs, (E) there exists one single FUPO, or any combination of (B) through (E). Dots on the MFPM shaft represent MPs, and spatial extents of measurable FUPO FPs are illustrated as cylinders.

1.1 Basics of ICA

In this section, basic concepts of ICA are outlined. The presentation is based on [2,3,13]. The strength of ICA lies in its ability to extract I ICs \mathbf{x}_i , $i = 1, 2, \dots, I$, from J measured signals \mathbf{y}_j , $j = 1, 2, \dots, J$, $I \leq J$. A measured signal is assumed to be a linear combination of the ICs, $\mathbf{y}_j = a_{1j}\mathbf{x}_1 + \dots + a_{Ij}\mathbf{x}_I$, $j = 1, 2, \dots, J$, where a_{ij} are coefficients of the linear combinations. Here, the measured signal \mathbf{y}_j is a column vector of N voltage samples taken via one channel of several simultaneously recorded MFPM channels. In matrix form $\mathbf{Y} = \mathbf{XA}$, where measurement vectors are the columns of \mathbf{Y} , \mathbf{X} consists of ICs in columns, and \mathbf{A} is a I -by- J mixing matrix with elements a_{ij} , $i = 1, 2, \dots, I$, $j = 1, 2, \dots, J$. The task of ICA is now to esti-

mate \mathbf{A} , given \mathbf{Y} , so that columns of \mathbf{X} are independent. In order to find J ICs, at least J simultaneously recorded channels must be available. Here, $I = J = 2, 3$. Thus, ICA requires that each MFPM channel records a *linear* combination of the FUPO FPs, which is valid, at least if the electric properties of the matter surrounding the FUPOs, and the measurement channels are constant during the measurement period, and the measured signals depend linearly on the actual FUPO FPs. Assumptions of ICA include that 1) the components are independent, and 2) the ICs have non-Gaussian distributions. The first assumption is the essence of ICA. ICs are the maximally non-Gaussian components, and with Gaussian components, ICA is impossible. The ambiguities of ICA are that 1) energies of the found ICs cannot be determined, and 2) order of ICs is undetermined. In the sequel, ICA calculation using, e.g., two signals y_n and y_m is denoted by $\text{ICA}(y_n, y_m)$, and the subscript of y denotes the number of the MP seen in Fig. 2.

Here, we use a fast iterative algorithm, FastICA [3,13], available for MATLAB (MathWorks Inc., Natick, MA, USA) from the FastICA WWW site [14]. Advantages of FastICA include fast convergence, no need to set a step size parameter, tuning with respect to data by selecting a non-linearity present for the calculations [13], and one by one (as in projection pursuit) or in parallel estimation of the ICs. On the average, computing FastICA on two of our 1250-point input signals took less than 10 ms of processor time on a 2.4 GHz Pentium IV processor. For most of our signals FastICA converged in less than 20 iterations, but we also encountered MFPMs for there was no converge. In such cases, turning on stabilization or using a different non-linearity in FastICA, or changing the number, length, or sampling rate of the input signals, or reducing noise, may result in convergence.

2. MULTIELECTRODE FP MEASUREMENTS

Measurements presented in this paper were originally made for epilepsy research to be published elsewhere. The measurement setup is illustrated in Fig. 2, and the considered MFPM signals are shown in Fig. 3. The methods used in the experiments were approved by the Provincial Government of Eastern Finland (approval number 99–61). The measurements presented in this paper are from one randomly selected rat out of a batch of 25 anaesthetized Kuopio Wistar rats. In a stereotactic instrument, a 16-channel silicon probe (courtesy of University of Michigan Center for Neural Communication Technology) with 100 μm MP separation was inserted via a drilled bone window. Recordings were made via 14 channels along the hippocampal subfields to monitor principal cell layers of dentate gyrus (DG) and Cornu Ammonis layer 1 (CA1), as well as CA1 Schaffer collaterals (Sch). Measurements via Channels 6, 8, and 15, seen in Fig. 3, were selected for demonstrating the proposed analysis, as they best exhibited the known characteristics of the above target cell layers. Positioning of the ME was observed from polarity of the FPs, firing patterns and population

spike shapes [15], and their latencies. Two stainless steel watch screws screwed to bone above the cerebellum served as indifferent and ground electrodes. The MFPM signals were 500-fold amplified, high-pass filtered at 0.1 Hz, low-pass filtered at 5 kHz, digitized to 16-bits at 12.5 kHz sampling rate, and stored to a personal computer (PC).

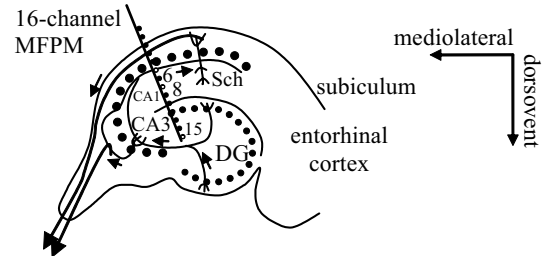


Fig. 2. Schematic illustration of the rat hippocampus –3.6 mm posterior to bregma, including an illustration of the recording electrode. Open circles on the electrode shaft illustrate the channels used in ICA, with Channel 6 in Cornu Ammonis layer 1 (CA1) pyramidal cell layer, Channel 8 amongst Schaffer collaterals (Sch), and Channel 15 in dentate gyrus (DG). Lines within the hippocampus illustrate fascicle, and dots the cellular layers. Cornu Ammonis layer 3 (CA3) location is also indicated.

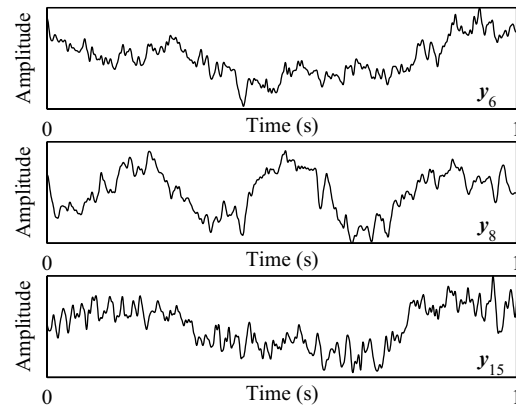


Fig. 3. One second of MFPMs from the rat hippocampus, measured simultaneously via Channels 6, 8, and 15, denoted by y_6 , y_8 , y_{15} , respectively.

In a PC, the sampling rate was lowered to 1250 Hz, and the signals were band limited within 0 Hz to 200 Hz in three steps: the signals were decimated by five, lowpass filtered using the 10th order Chebyshev type II filter with stopband ripple 60 dB down and cutoff stopband edge frequency set to 200 Hz, and decimated by two. The employed decimation function included an appropriate low-pass filter. The lowpass filtering was performed both forward and backward to preserve signal phase. Limiting the frequency band of interest below 200 Hz allows us to concentrate on FPs, and to exclude action potentials.

3. SIGNAL ANALYSIS METHODS

In this Section, the applied signal analysis methods are given. For frequency analysis, power spectral densities

(PSDs) were calculated using the Welch's method [16], with 1250-sample signals padded with zeros [17] to the length of 65536, and a window of 16384 samples in order to achieve sufficient reverberation peak frequency detection. The window was moved eight samples at a time.

To analyze the ICs, similarities between the ICs from different ICA calculations are to be determined. Here, two approaches are demonstrated: hierarchical clustering [18], and correlation analysis [19]. Hierarchical clustering produces disjoint sets of ICs, so that the ICs assigned to one cluster are more similar to each other, here, in the sense of correlation distance. A cutoff point was decreased until more than one cluster was found. This may underestimate the number of clusters, but it is otherwise hard to set the cutoff point objectively. Also, correlation analysis yields a similarity measure between all the ICs, thus allowing one to analyze the extent of FUPOs contributing to each IC. Correlation analysis can also be used in cluster validation. In correlation analysis, pair wise cross-correlations between all the ICs were calculated and the time lags of the maximum correlations were recorded. Ambiguity of the IC sign presents a problem in the delay analysis; if the similar ICs are in opposite phases, the apparent time lag is modified by half the signal period. Thus, correlations are calculated with both signs of one IC, and the shorter of the found time lags is reported.

4. RESULTS OF ICA OF RAT HIPPOCAMPAL FPS

In this section, results of the described MFPM ICA calculations are given, with some exemplary hippocampal FUPO analyses. It is to be noted that the shown examples are too few to deduce the true operation of the hippocampus. In Fig. 4A, the ICAs calculated with all combinations of two or three of the signals seen in Fig. 3, are shown along with the clustering results. PSDs of the ICs in Fig. 4A are shown in Fig. 4B.

Let us first look at the clustering results without reference to anatomy. With all the combinations of the signals in Fig. 3 as inputs, ICA produced the ICs seen in Fig. 4A, and the clustering grouped the ICs into three clusters. The clustering of ICs in Fig. 4, agrees fairly well with visual intuitive inspection both in time and frequency domains. Only IC₁₂ differs notably from the other ICs in Cluster 3. Also, observing the frequencies of the PSD peaks in Table 1, it is seen that the PSD peak frequencies within each cluster are fairly similar; PSDs of Cluster 1 ICs contain only one peak at around 3Hz, Cluster 2 PSDs have three peaks at 0.8 Hz, 3.1 Hz, and 4.5 Hz, and Cluster 3 PSDs have a common peak at a little over 1 Hz. From the correlation coefficients in Table 2, it is seen that IC₁₁ correlates strongly with IC₃₁ and IC₄₁. Likewise, IC₃₁ correlates strongly with IC₄₁, as it should. These correlations agree with the clustering result for Cluster 1. Furthermore, it is seen from Table 2 that the maximum correlation between IC₁₁, IC₃₁, and IC₄₁ is found at zero time lag, and Cluster 2 is seen to be confirmed by strong correlation of C₂₂ and IC₄₃, whose maximum correlation occurs at zero time lag.

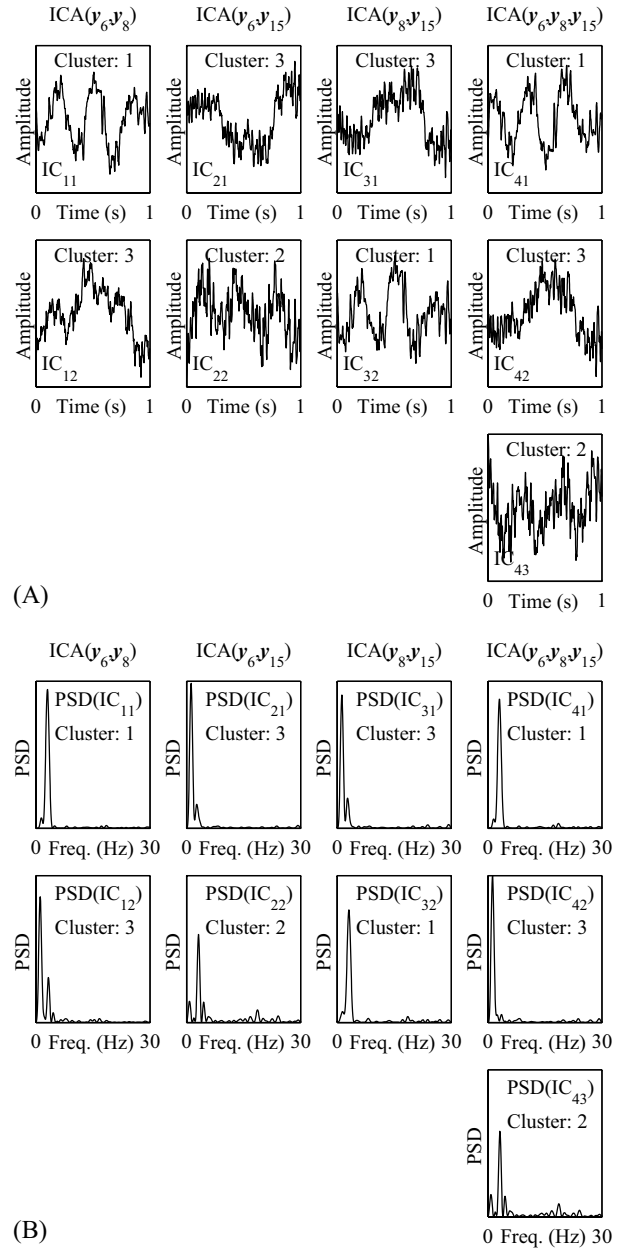


Fig. 4. (A) ICAs of two to three signals seen in Fig. 3. ICs from different ICAs are shown in columns, and individual ICs are labeled for later reference. Also shown are the IC clustering results. (B) PSDs of the ICs seen in (A). The amplitude range is equal for all the subplots in (A), and likewise the PSD range in (B).

Table 1. Frequencies (Hz) of the PSD peaks in Fig. 4B, which are above 10 % of the maximum PSD over all the PSDs in Fig. 4B. Also, the cluster assignments (CL), seen in Fig. 4, are shown.

PSD(IC ₁₁), CL 1	PSD(IC ₂₁), CL 3	PSD(IC ₃₁), CL 1	PSD(IC ₄₁), CL 1
3.1	1.2 2.7	3.1	3.0
PSD(IC ₁₂), CL 3	PSD(IC ₂₂), CL 2	PSD(IC ₃₂), CL 3	PSD(IC ₄₂), CL 3
1.1 3.3	0.8 3.1 4.5	1.3	1.2
			PSD(IC ₄₃), CL 2
			0.8 3.1 4.5

To associate the ICs in Fig. 4A with neural FUPOs, it is noted that Cluster 1 ICs appear when the measurement y_8

participates in ICA. Referring to Fig. 2, this suggests that Cluster 1 like activity is associated with Sch FUPO, with one prominent reverberation component at around 3 Hz, c.f., Table 1. Cluster 2 ICs occur when both measurements y_6 and y_{15} participate in ICA, which suggests that CA1 and DG participate in the same FUPO (CA1/DG FUPO). From Table 1 the CA1/DG FUPO is seen to carry three frequency components: 0.8 Hz, 3.1 Hz, and 4.5 Hz. From Table 2 it is also seen that Cluster 2 ICs correlate strongly and are in phase with each other. Finally, a Cluster 3 IC is present in all ICAs, i.e., Cluster 3 ICs represent a signal component, which is present in all the considered hippocampal structures, and carry a frequency component at a little over 1 Hz, and in two cases also a component around 3 Hz. From Table 2 it is seen that Cluster 3 is bound together by much weaker correlations than the other clusters. Observing the lower correlations in Table 2, the Cluster 2 ICs, IC₂₂ and IC₄₃, are seen to weakly correlated with the Cluster 1 ICs, IC₁₁, IC₃₁, and IC₄₁, with the Cluster 2 ICs preceding the Cluster 1 ICs by 107 ms. This suggests that Sch FUPO activity is related to the CA1/DG FUPO activity, but lags a little over 100 ms behind.

Table 2. Time lags of maximum correlations in milliseconds (upper values), and correlation coefficients r (lower values) for all pairs of ICs in Fig. 4A, whose $r < 0.56$ (or $p < 0.0001$). For example, the strongest correlation between IC₄₁ and IC₄₃ in Fig. 4A is observed when IC₄₁ lags 107 ms behind IC₄₃.

	IC ₁₂	IC ₂₁	IC ₂₂	IC ₃₁	IC ₃₂	IC ₄₁	IC ₄₂	IC ₄₃
IC ₁₁			-107 0.8936	0 0.9997		0 0.9992		-107 0.8868
IC ₁₂		0 0.9523			-1 0.9314		0 0.9449	
IC ₂₁				0 0.9917		0 0.9912		
IC ₂₂				107 0.8882		107 0.8839		0 0.9998
IC ₃₁						0 0.8814		-107 0.8814
IC ₃₂							0 0.9986	
IC ₄₁								-107 0.8772
IC ₄₂								

5. CONCLUSIONS AND DISCUSSION

In this paper, we have described a method for analyzing NPs from MFPMs using ICA. The proposed method provides new means for analyzing functioning of neural networks, and may be applied to any most ME measurement. The basic requirement for applying ICA is that a number of simultaneously measured signals carry linear combinations of the original source signals, i.e., FUPO FPs. This is generally well satisfied by most MFPM measurements, at least if the distance between MPs is sufficiently small. The proposed method was demonstrated by ICA of MFPMs from the rat hippocampus. Exemplary hippocampal FUPOs were deduced from ICA results and frequency contents of ICs were analyzed.

In order to draw correct conclusions about the FUPOs, or the neural operational modes, and thus to deduce the functioning of the target brain structure, ICA finding must be carefully related to the neuroanatomy. Although, from information-theoretic point of view, ICs might be interesting by the virtue of their existence. Regardless whether the ICs are interpreted as FUPOs or neural operational modes, they may yield information on the information coding, flow and processing in the brain.

ACKNOWLEDGEMENTS

J. M. A. Tanskanen's work has been funded by Academy of Finland (decision number 80323). J. E. Mikkonen's work has been partially funded by Finnish Cultural Foundation, and by Kuopio University Fund.

REFERENCES

- [1] A. Hyvärinen, "Survey on independent component analysis," *Neural Computing Surveys*, vol. 2, pp. 94–128, 1999. Available: <http://www.cis.hut.fi/aapo/papers/NCS99web/>.
- [2] A. Hyvärinen and E. Oja, "Independent component analysis: algorithms and applications," *Neural Networks*, vol. 13, pp. 411–430, 2000.
- [3] A. Hyvärinen, J. Karhunen, and E. Oja, *Independent Component Analysis*. New York, NY, USA: John Wiley & Sons, 2001.
- [4] J. V. Stone, "Independent component analysis: an introduction," *Trends in Cognitive Sciences*, vol. 6, pp. 59–64, Feb. 2002.
- [5] A. Metin, Ed., *Time Frequency and Wavelets in Biomedical Signal Processing*. New York, NY, USA: IEEE Press, 1997.
- [6] J. A. Freeman and C. Nicholson, "Experimental optimization of current source-density technique for anuran cerebellum," *J. Neurophysiology*, vol. 38, pp. 369–382, 1975.
- [7] L. Zhukov, D. Weinstein, and C. Johnson, "Independent component analysis for EEG source localization," *IEEE Eng. Med. Biol.*, pp. 87–96, May/June 2000.
- [8] R. Vigário, J. Särelä, V. Jousmäki, M. Hämäläinen, and E. Oja, "Independent component approach to the analysis of EEG and MEG recordings," *IEEE Trans. Biomed. Eng.*, vol. 47, pp. 589–593, May 2000.
- [9] T.-P. Jung, S. Makeig, M. J. McKeown, A. J. Bell, T.-W. Lee, and T. J. Sejnowski, "Imaging brain dynamics using independent component analysis," *Proc. IEEE*, vol. 89, pp. 1107–1122, July 2001.
- [10] K. Kobayashi, C. J. James, T. Nakahori, T. Akiyama, and J. Gotman, "Isolation of epileptiform discharges from unaveraged EEG by independent component analysis," *Clinical Neurophysiology*, vol. 110, pp. 1755–1763, 1999.
- [11] M. Laubach, M. Shuler, and M. A. L. Nicolelis, "Independent component analysis for quantifying neuronal ensemble interactions," *J. Neuroscience Methods*, vol. 94, pp. 141–154, 1999.
- [12] G. D. Brown, S. Yamada, and T. J. Sejnowski, "Independent component analysis at the neural cocktail party," *Trends in Neurosciences*, vol. 24, pp. 54–63, Jan. 2001.
- [13] A. Hyvärinen, "Fast and robust fixed-point algorithms for independent component analysis," *IEEE Trans. Neural Networks*, vol. 10, pp. 626–634, May 1999.
- [14] FastICA Package for Matlab. Available from <http://www.cis.hut.fi/projects/ica/fastica/>. Helsinki University of Technology: Espoo, Finland, 2003.
- [15] H. Markram, J. Lübke, M. Frotscher, and B. Sakmann, "Regulation of synaptic efficacy by coincidence of postsynaptic APs and EPSPs," *Science*, vol. 275, pp. 213–215, Jan. 1997.
- [16] M. H. Hayes, *Statistical Digital Signal Processing and Modeling*. New York, NY, USA: John Wiley & Sons, 1996.
- [17] L. B. Jackson, *Digital Filters and Signal Processing with MATLAB Exercises*. Boston, USA: Kluwer Academic Publishers, 1996.
- [18] D. Hand, H. Mannila, and P. Smyth, *Principles of Data Mining*. Cambridge, MA, USA: MIT Press, 2001.
- [19] J. S. Milton and J. C. Arnold, *Introduction to Probability and Statistics*. New York, NY, USA: McGraw-Hill, 1995.